Applied Physics A (2018) 124:810
https://doi.org/10.1007/s00339-018-2171-7

Applied Physics A
Materials Science & Processing

Characterization of nano-crystalline Ti–W–N thin films for diffusion barrier application: a structural, microstructural, morphological and mechanical study

Reza Jalali[1] · Mojtaba Parhizkar[1] · Hassan Bidadi[1] · Hamid Naghshara[1] · Mohamad Javad Eshraghi[2]

Received: 30 May 2018 / Accepted: 8 October 2018 / Published online: 11 November 2018
© Springer-Verlag GmbH Germany, part of Springer Nature 2018

Abstract
Ti–W–N thin films with various W contents are deposited on the glass and 304 steel substrates, kept at 150 °C, using the reactive magnetron co-sputtering system. The films were deposited with simultaneous sputtering of Ti and W targets where they powered by DC and RF sources, respectively. The effect of W content on the structure, microstructure and mechanical properties of Ti–W–N thin films are investigated by X-ray diffraction (XRD), field emission scanning electron microscopy, energy-dispersive X-ray spectroscopy (EDX), atomic force microscopy (AFM) and nanoindentation tester. The results show that all films have NaCl-type structure with (200) or (111) preferred orientation, depending on the W content. Furthermore, cross-sectional images corroborate the formation of columnar structure and reduction in distance between the columns with increasing W content. The grains' size calculated from XRD patterns and SEM micrographs revealed that increasing W content results in increasing their values in the films. Study of the surface morphology and the surface roughness of the films confirm the increase of surface roughness as a function of W content, and this is in agreement with the increase seen in the grain size. Incorporation of W to Ti–N system results in dramatic reduction in electrical resistivity. Addition of W to the films has significant effects on the film stoichiometry. With increasing RF power, the hardness of the films increases and reaches a maximum value of about 26.5 GPa at a RF power of 80 W while in higher values of power the hardness decreases.

1 Introduction

Copper, Al, and Au as the metallization materials in semiconductor devices react with Si at processing temperatures, so the use of a diffusion barrier between Si and metallization is necessary to prevent interface reactions and device failure. A good barrier layer is characterized by high thermal and chemical stability, good adhesion and low electrical resistivity. Tungsten-based films have been widely used in various barrier applications due to special properties of W such as its very high melting point (3407 °C). For a long time, Ti–W alloys were investigated and used as a diffusion barrier, however, they showed low failing temperatures as low as 300–350 °C [1]. Introducing nitrogen into Ti–W layers and formation of Ti–W–N leads to a higher stability of microstructure and higher density of interface, and consequently, a good barrier performance [2]. Dirks et al. [3] reported that heating of Ti–W–N thin films at 450–500 °C did not show any significant change in interfacial structure. High hardness, good adhesion, and excellent corrosion resistance have caused Ti–W–N thin films to be widely used in resistance transmitters and cutting tools [4–6]. In addition, due to the formation of magneli phase (WO_3) on the top of Ti–W–N films, these layers had the ability to reduce friction coefficient by adapting self-lubrication [7]. Most of the investigations conducted on Ti–W–N thin films are focused on the effect of N_2 partial pressure on the properties of Ti–W–N thin films [8–13] which concluded improvement of mechanical behavior with increasing N_2 partial pressure to a critical value. Probably, the only study that has been dedicated to the study of W content effect on the properties of these films was conducted by Moser et al. [14] who grew single phase $Ti_{1-x}W_xN$ thin layers with $0 \leq x \leq 0.7$ at a substrate temperature of 500 °C. They found that the transition of preferred orientation from (111) to (002) occurs at x between 0.1 and

✉ Mojtaba Parhizkar
parhizkar@tabrizu.ac.ir

[1] Department of Condensed matter, Faculty of Physics, University of Tabriz, 29 Bahman Blvd., Tabriz, Iran

[2] Department of Semiconductors, Materials and Energy Research Center (MERC), Karaj, Iran

0.2 and by TEM analysis it was revealed that all prepared films have a columnar structure.

However, in W-based films with columnar structures, related grain boundaries can act as fast diffusion paths. This shows that the structure and microstructure of these films have a significant role in their barrier properties [15]. Furthermore, in many cases, preparation of Ti–W–N thin films using DC or RF sputtering systems were done by sputtering of binary Ti–W targets with different composition ratios; in this situation, possibility of accurate control of film composition reduces [2, 4, 5, 16–18]. Due to lack of enough knowledge about the effect of W content and the use of separate Ti and W targets on properties of Ti–W–N thin films at substrate temperatures lower than 500 °C, the aim of the present work is to prepare Ti–W–N thin films, with simultaneously sputtering of Ti and W targets, with various W contents at a substrate temperature of 150 °C and investigate their properties and finally, finding the layer with best electrical, mechanical, microstructural and structural properties for an application as diffusion barrier.

2 Materials and methods

Deposition of Ti–W–N thin films onto the glass and 304 steel substrates was carried out using a dual (DC & RF) reactive magnetron sputtering system. This system was evacuated with a turbo-molecular pump along with a rotary pump, to a base pressure of 5×10^{-3} Pa. After introducing Ar and N_2 as sputtering and reactive gases, respectively, to the chamber, working pressure for deposition process reached 2×10^{-1} Pa. Before being placed in the chamber, substrates were ultrasonically cleaned with acetone, alcohol, and twice with deionized water and dried with compressed air. Also, steel substrates were polished before being cleaned ultrasonically. For deposition of Ti–W–N thin films, two pure metallic Ti and W targets (99.99% purity) with 3″ diameter were simultaneously sputtered in an Ar–N_2 environment, so that Ti target was powered by DC power supplier and W target by RF source. For all deposition processes, the DC power for Ti target was fixed at 250 W and for having different amounts of W in prepared films, RF power (P_{RF}) for W target varied from 0 to 100 W (0 W, 20 W, 35 W, 50 W, 65 W, 80 W and 100 W). Before deposition process, both targets were pre-sputtered for 30 min in the presence of shutter to remove any contaminations from their surface. Ar and N_2 flow rate were fixed at 18 and 1.31 sccm, respectively, and during the whole deposition process, their flow rate was controlled by mass flow controllers. Ti–W–N thin films were deposited onto the substrates at a temperature of 150 °C. To increase the substrate temperature to 150 °C, two 500 W pen-shaped filamentary lamps were placed parallel on top of the substrates. The distance between targets and the substrates was 180 mm and the thickness of the deposited films was constant at about 150 nm.

The structure and phase composition of the films were analyzed by X-ray diffraction (XRD: D500, Siemens) over a 2θ range of 20°–80°, using a Cu Kα wavelength (1.5406 Å). The microstructure and cross-section images of the deposited films were investigated using field emission scanning electron microscopy (FE-SEM, MIRA3, Tescan). To understand the elemental composition of Ti–W–N thin films grown at various W contents, an energy-dispersive spectrometer (EDS) that was coupled to FE-SEM equipment was used. The surface and roughness of deposited films were characterized by an atomic force microscope (Auto probe CP, Park Scientific Instruments, USA) in contact mode. Hardness and elastic modulus of the Ti–W–N films were determined by means of a nanoindentation tester (Triboscope system, Hysitron Inc. USA) with a Berkovich indenter tip, at room temperature. The applied loading force was 75 μN, and to ensure the reliability of the results, measurements were repeated five times for each sample. Also, the electrical resistivity of the prepared films was measured by a four point probe equipment.

3 Results and discussion

3.1 Structural analyses

Figure 1 shows the XRD patterns of the deposited Ti–W–N thin films with different W target powers. It can be seen from the figure that all deposited films have peaks related to crystalline structures. For the film without W, there is only a single peak at 43.2° that refers to (200) Ti–N phase. Low intensity and broadening of this peak represents low crystallinity of this film, which can be related to low nitrogen flow rate [19]. After introducing W to Ti–N structure, another peak was formed at 37.1° corresponding to (111) plane. Taking into account the standard reference sample listed in (01-087-0633) and (00-025-1257) PDF databases, the films can be assigned to TiN/W_2N phase in fcc–NaCl structure. By increasing the power of W target, the intensity of both peaks increases and the peaks become sharper, which indicate the improvement of crystallinity. When RF power reaches 50 W, the (220) peak of TiN/W_2N phase can be identified at 62.3°, and as RF power increases further to 65 W and 80 W, the intensity of peaks increases; finally, at an RF power of 100 W, another peak at 74.4° is formed, which can be indexed as (311) plane of TiN/W_2N phase.

As shown in Fig. 1, generally, with increasing RF power from 0 to 100 W, peaks are shifted to lower angels. Corresponding *d*-values calculated from Bragg's law indicate a reverse change relative to changes of peak positions so that with increasing RF power from 0 to 100 W, as listed in

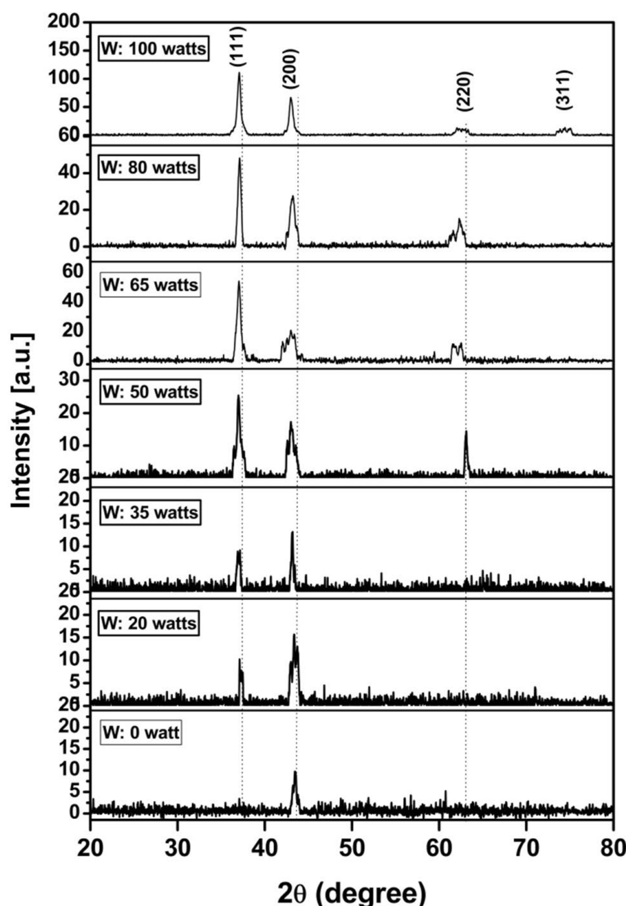

Fig. 1 XRD patterns of Ti–W–N thin films with different W contents

Table 1 Variation of calculated *d*-values (200) plane and lattice constants as a function of W target power

W target power (W)	*d*-value (A°)	Lattice constant (A°)	
		Experimental	Theoretical
0	2.081	4.161	4.176
20	2.085	4.170	4.178
35	2.093	4.186	4.184
50	2.103	4.205	4.21
65	2.097	4.195	4.188
80	2.091	4.182	4.168
100	2.103	4.205	4.156

Table 1, *d*-values corresponding to (200) peak are gradually increased. Variation of peak positions, and as a result, corresponding *d*-values with introducing W to the Ti–N structure can be attributed to the changes in lattice microstrain, nitrogen content or stoichiometry, material defects and defective structures of the films [20, 21], as will be discussed below.

The experimental lattice constant (a) of the deposited Ti–W–N thin films with different W contents was calculated from Eq. (1).

$$d_{hkl} = \frac{a}{\sqrt{h^2 + k^2 + l^2}}, \tag{1}$$

where (hkl) are the Miller indices of diffraction planes and d_{hkl} is the d-value calculated from Bragg's law. Calculation of lattice parameters using Eq. (1) shows that with increasing RF power from 0 to 50 W, the lattice parameter increases from 4.18 to 4.21 Å and then with further increase of RF power up to 100 W, it decreases to about 4.19 Å. These values are not in good agreement with the values of 4.23 Å, 4.24 Å and 4.235 Å reported in [4, 18] which can be related to sub-stoichiometric properties of deposited films due to the low nitrogen flow rate. Moreover, changes in the stress state due to the substitution of Ti by W atoms can affect the lattice parameters [20]. With regard to the results obtained from XRD patterns, it can be concluded that Ti–W–N thin films are solid solutions composed of two Ti–N and β-W_2N phases, which is in agreement with the results reported in the literature [4, 21]. According to this, the theoretical lattice parameters of Ti–W–N films were calculated using the Vegard's law (Eq. 2) [22]. For solid solutions, Vegard's law predicts a linear dependence of lattice parameter on composition.

$$a_{\mathrm{Ti}_{(1-x)}W_xN} = (1-x)a_{\mathrm{Ti}N} + xa_{W_2N}, \tag{2}$$

where $a_{\mathrm{Ti}_{(1-x)}\mathrm{W}_x\mathrm{N}}$, a_{TiN} and a_{W_2N} are the lattice parameters of Ti–W–N, Ti–N and W_2N, respectively. The parameters a_{TiN} and $a_{\mathrm{W_2N}}$ were extracted using the (01-087-0633) and (00-025-1257) PDF cards, respectively, and the compositional results obtained from energy-dispersive X-ray spectroscopy (EDX) were used (Table 3). Table 1 shows the obtained results based on the experiment and theory. As can be seen, both results have the same trend. Initially, by increasing RF power from 0 to 50 W, the lattice parameter increases, and from 50 to 100 W, it decreases. It seems that the observed difference between the results obtained from two methods can be related to the difference between the stoichiometry of the prepared films and materials considered in PDF cards.

The effect of W content on the coating texture can be better described by calculating the texture coefficients. The texture coefficients (T) of the prepared Ti–W–N thin films at different RF powers were calculated from the corresponding peaks of XRD patterns using Eq. (3).

$$T = I(hkl)/[I(111) + I(200) + I(220) + I(311)], \tag{3}$$

where $I(hkl)$ indicates the (111), (200), (220) or (311) orientation. The films prepared at lower RF powers (< 50 W) show the (200) preferred orientation; however, those prepared at higher powers ($\geqslant 50$ W) have the preferred orientation of

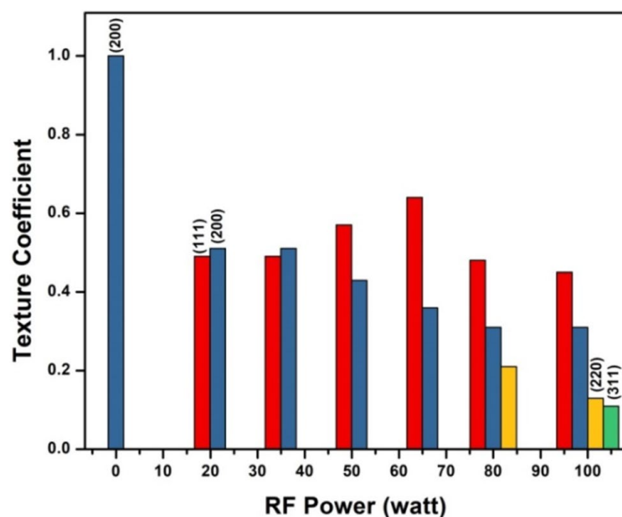

Fig. 2 Texture coefficients of deposited Ti–W–N thin films at different RF powers

(111) as shown in Fig. 2. The preferred orientation of the films was determined by the competition between strain and surface energies. Finally, the process of energy minimization causes the preferred orientation to occur in the direction of the plane that has the minimum total free energy compared to other planes [23]. As mentioned in the literature [24–26], Ti–N thin films can have (111) or (200) preferred orientation depending on the deposition conditions. Arshi et al. [27] reported that in Ti–N films, the (111) plane has the minimum strain energy and the (200) plane has the minimum surface energy. Comparing with the mentioned work, probably low substrate temperature results in low surface energy in the prepared Ti–N thin film and those in which Ti–N is the dominant phase ($P_{RF} < 50$ W). At lower RF powers (< 50 W), it can be concluded that the effect of surface energy is the most effective factor in the formation of the preferred orientation. According to compositional analyses, presented in the following sections, by increasing RF power (⩾50 W), the role of W_2N phase becomes more dominant. W_2N thin films may show (111) or (200) preferred orientation, depending on deposition conditions. Addonizio et al. [28] reported that in the range 7.7–20% of nitrogen concentration in argon/nitrogen atmosphere and 300–900 W discharge power applied to the W target, prepared W_2N thin films show the (111) preferred orientation. Wen et al. [29] showed that at low substrate bias voltages, W_2N thin films have a (200) preferred orientation. Therefore, in Ti–W–N thin films prepared without substrate bias and with dominant W_2N phase, it is expected that the (111) plane is the preferred orientation.

For calculation of the average grain size and lattice strain, the Williamson–Hall method was used, which is given in the following formula [30]:

$$\frac{\beta \cos\theta}{\lambda} = \frac{0.9}{D} + \frac{4\varepsilon \sin\theta}{\lambda}, \quad (4)$$

where β is the instrumental corrected full width at half maximum (FWHM), θ is Bragg's angle, D is the average grain size, ε is the lattice strain and λ is the X-ray wavelength with Cu K_α radiation (1.5406 Å). The average grain size and lattice strain of the films can be obtained from the intercept and slope of the Williamson–Hall plot, respectively. Because of the presence of only one peak for Ti–N film, the Scherrer formula ($D = 0.9\lambda/\beta\cos\theta$) was used for calculating the grain size. The results are summarized in Table 2. As can be seen from Table 2, by increasing RF power from 0 to 65 W, the grain size increases and with further increase in RF power to 100 W, it decreases. In this work, the grain size can be affected by several factors such as substrate temperature, W content, the kinetic energy of sputtered particles, lattice strain and stress.

A substrate temperature of 150 °C leads to high mobility of the adatoms through thermal vibrations and low number of nucleation points resulting in the generation of larger grains [18, 31, 32]. As previously reported [18], increasing the substrate temperature up to a specified value leads to an increase in the grain size of the Ti–W–N thin films. By increasing RF power from 0 to 100 W, the number of small W atoms ($r_W = 210$ pm) that replace larger Ti atoms ($r_{Ti} = 215$ pm) is increased, thus the grain size is expected to decrease with increasing W content (contrary to what has been observed in experience).

Increasing RF power from 0 to 100 W leads to sputtered particles that collide with substrate with higher energy. Consequently, some defects may be formed on the surface of the films. These defects act as re-nucleation sites and reduce the size of grains [33]. The grain boundaries are defects with high energy, and grain growth eliminates the grain boundary area and leads to a reduction in free energy of the system. Competition between the elimination of Gibbs free energy and strain energy leads

Table 2 Resistivity, lattice strain and the grain size of the prepared Ti–W–N thin films

Sample	W target power (W)	Resistivity (kΩ cm)	Lattice strain	Grain size (nm)	
				SEM	XRD
1	0	3.00	–	18.0	5.3
2	20	0.748	0.286	20.1	8.66
3	35	0.782	0.299	20.6	10.1
4	50	0.385	0.281	21.9	14.0
5	65	0.247	0.288	21.7	19.8
6	80	0.187	0.007	22.4	13.9
7	100	0.063	0.010	22.6	16.3

to an equilibrium grain size. Londono-Menjura et al. [18] reported that by decreasing lattice microstrain, the grain size decreases. It can be observed that the grain size is significantly affected by the variation of lattice microstrain and the energy of sputtered particles.

The electrical resistivity of the films decreased from 3.00 to 0.063 kΩ cm as a function of RF power, as shown in Table 2. This can be due to the fact that with increasing RF power the number of sputtered W atoms within the chamber increased but because of a low flow rate of nitrogen gas (1.31 sccm), all the W atoms cannot interact with N_2 molecules and participate in the film's composition as W atom, not as W–N phase. On the other hand, with regard to increasing of grain size with increasing RF power, the number of the grain boundary and as a result boundary states that resist against electrical carrier movement decrease which can be another reason for reducing electrical resistivity.

3.2 Microstructural analyses

The FE-SEM and cross-sectional morphologies of Ti–W–N thin films prepared with different RF powers are presented in Figs. 3, 4. In the absence of W, a porous microstructure without special grain shape can be observed (Fig. 3a). When tungsten is added to the film, it can be noticed that the microstructure transits to a triangular grain (Fig. 3b). Further increase in RF power to 65 and 80 W causes the films to become denser, and at an RF power of 100 W, the distance between the grains approximately disappears, indicating that the films become more compact and denser with increasing W content in the structure of the films. Additionally, in a RF power of 100 W, the grain shape again becomes irregular (Fig. 3d). At a substrate temperature of 150 °C, some of the weaker bonds of nitrogen atoms can break, and these atoms may leave their positions and be released from the film. Therefore, defects such as voids and vacancies can be observed in these films [34]. On the other hand, sub-stoichiometric properties of the deposited films can be another

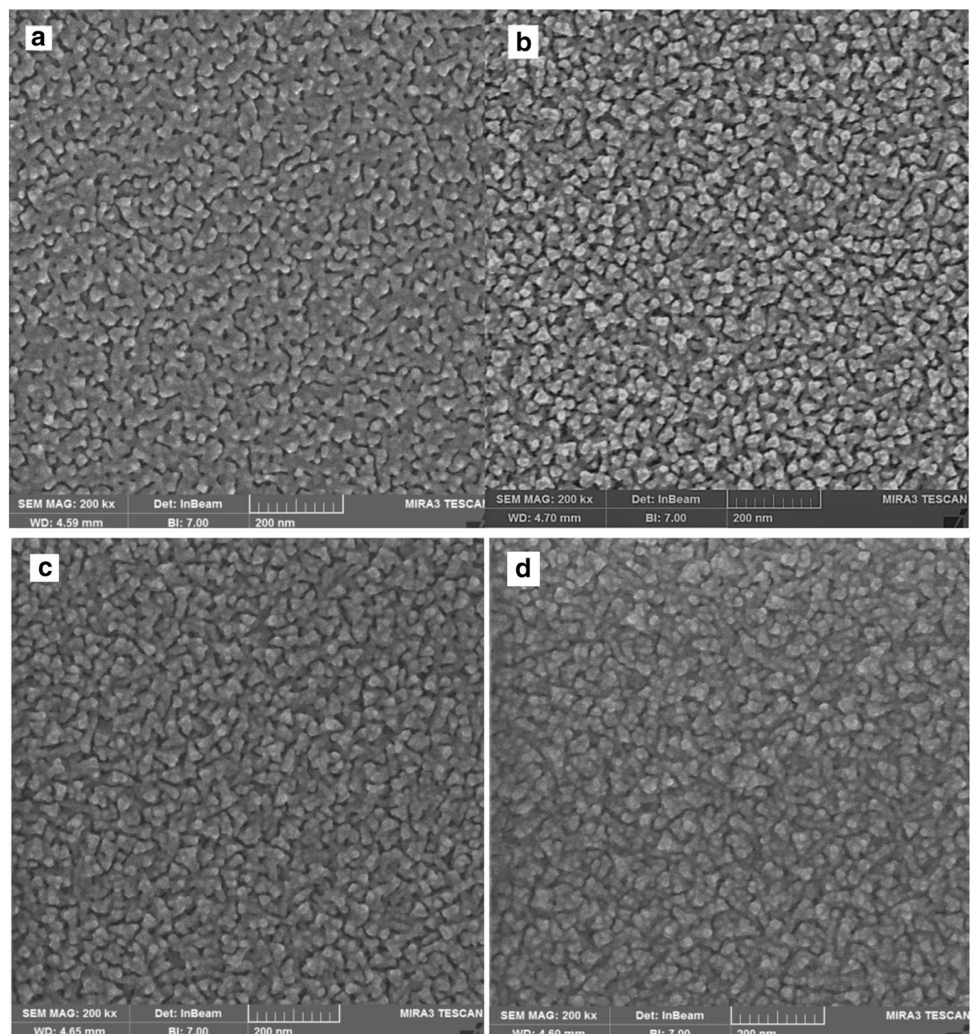

Fig. 3 FE-SEM micrographs of Ti–W–N thin films deposited using different RF powers **a** 0, **b** 35, **c** 65, **d** 100 W

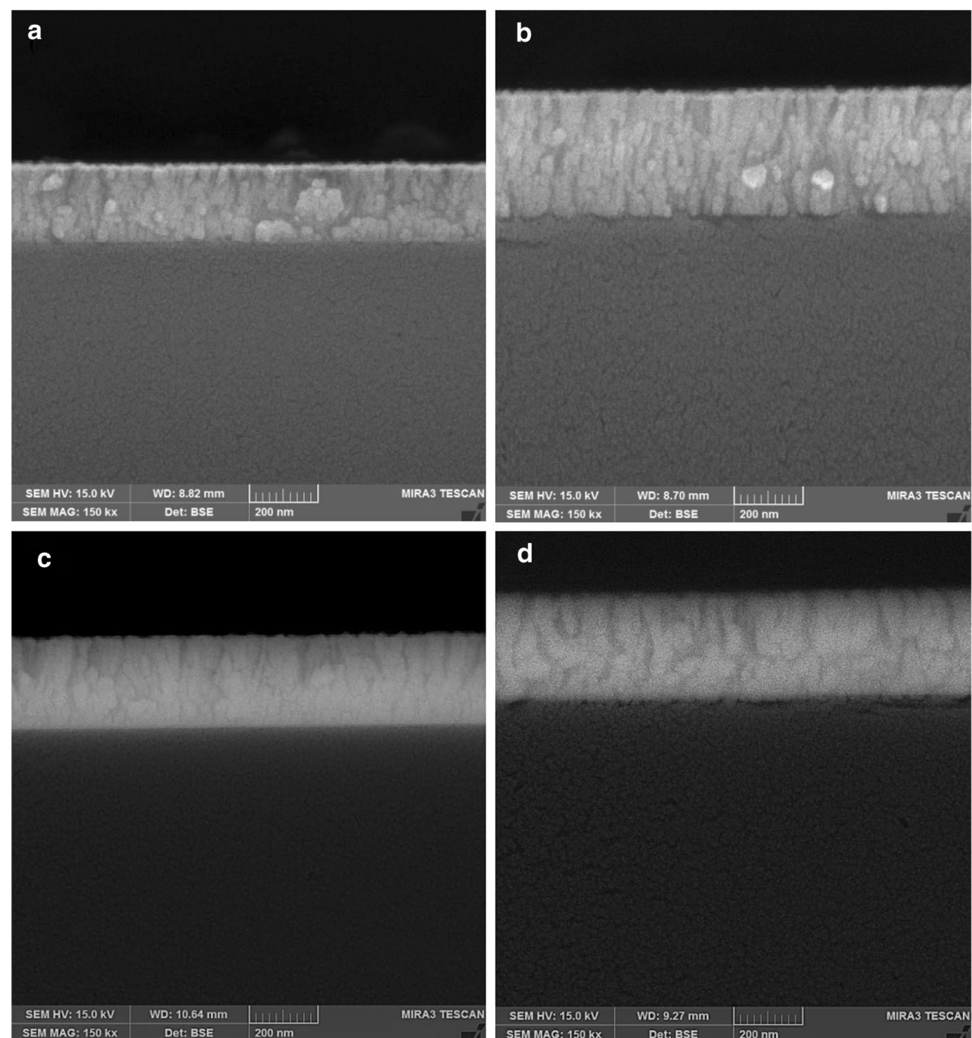

Fig. 4 FE-SEM cross-section images of Ti–W–N thin films prepared with different RF powers **a** 0, **b** 35, **c** 65, **d** 100 W

factor for this type of lattice defects. The presence of W can increase the covalent level of the bonding, and attractive forces among the columns leads to improvement in the compactness of the films [20].

Calculating average grain size from FE-SEM micrographs using Digimizer software shows that by increasing RF power from 0 to 100 W, the grain size is increased from 18.0 to 22.6 nm; moreover, the same trend is observed in XRD data. In this software, obtained grain size values were calculated from the average of 100 grain sizes in each film. The difference between the grain size calculated from XRD patterns and FE-SEM micrographs can be attributed to the non-spherical shape of the grains.

As can be seen from the FE-SEM cross-sectional images, all films have a columnar microstructure perpendicular to the interface. In the film without tungsten, columnar structure is not very clear, which can be attributed to its low crystallinity (Fig. 4a). When W is added to the Ti–N structure, columns can be identified clearly. Moreover, by increasing RF power to 65 W, the distance between the columns decreases (Fig. 4b, c). In the film prepared with 100 W RF power, a series of cracks can be seen that are distributed in the bulk of the film. These cracks do not seem to be the spacing between the columns (Fig. 4d). Therefore, it can be suggested that these cracks have arisen from the thermal stresses due to the existing difference in thermal expansion coefficients of the film components, $\alpha_{\mathrm{TiN}} = 9.36 \times 10^{-6}\,\frac{1}{K}$ [35] and $\alpha_{\mathrm{W_2N}} = 5.7 \times 10^{-6}\,\frac{1}{K}$ [36], and $\alpha_{\mathrm{glass}} = 8.5 \times 10^{-6}\,\frac{1}{K}$ for the glass substrate [37]. Regarding W_2N as the dominant phase of the film prepared with 100 W RF power, the presence of these cracks can be attributed to the existing difference between the thermal expansion coefficients of W_2N phase and glass.

Table 3 lists elemental composition of Ti–W–N thin films deposited with different RF powers. These compositions were determined using EDX micro-analyzer coupled to FE-SEM instrument. In all films, a very little amount of oxygen was detected. The results showed that by increasing RF power from 0 to 100 W, tungsten content increases from 0 to 58.25 at% and titanium content decreases from 53.34

Table 3 Elemental composition of Ti–W–N thin films prepared using different RF powers

Sample	Ti Power (W)	W Power (W)	Elemental composition (at %)			W/Ti (x)	Ti/W (x)	N/(Ti + W)
			Ti	W	N			
1	250	0	53.34	0	46.66	0	–	0.87
2	250	20	48.52	25.68	25.80	0.53	1.89	0.35
3	250	35	44.52	29.65	25.83	0.66	1.5	0.35
4	250	50	25.75	34.34	39.91	1.33	0.75	0.66
5	250	65	23.54	41.7	34.76	1.77	0.56	0.53
6	250	80	19.67	50.63	29.70	2.57	0.38	0.42
7	250	100	15.94	58.25	25.81	3.65	0.27	0.34

to 15.94 at% linearly in the composition of the films. This indicates that W atoms can replace Ti atoms. Furthermore, a substitutional solid solution is formed, where N can be in interstitial positions [20]. Similar results were reported in [4, 18]. The deposited Ti–N film has the highest nitrogen percentage and then by increasing W content in the film composition, nitrogen content decreases. This can be expected because of low affinity of W for N compared to Ti for N, which is justified by the higher formation energy of W–N bond (151 kcal/mol) compared to that of Ti–N bond (113.8 ± 8 kcal/mol) [38]. For all deposited films, N/(Ti + W) ratio is lower than the one that represents their sub-stoichiometric characteristic which is caused by low nitrogen flow rate.

Figure 5 shows the surface morphology of deposited Ti–W–N thin films with different RF powers in two- and three-dimensional forms. From Fig. 5a, it can be observed that the prepared Ti–N thin films have a smoother surface in comparison with those containing W in their structures. The results of surface roughness that is characterized by the root mean square (RMS) indicate that by increasing RF power, the roughness of the films increases (Fig. 6). Increasing the surface roughness as a function of W content is consistent with increasing the grain size values calculated from XRD patterns and FE-SEM micrographs. Consequently, by increasing RF power from 0 to 100 W, the RMS of the films increases from 2.65 to 4.98 nm. In addition to the above discussion about the grain size, low deposition rate at lower RF power can act as a factor that reduces surface roughness [39].

3.3 Mechanical analyses

For investigating the mechanical properties of some of the prepared Ti–W–N thin films deposited onto the 304 steel substrate, a triangular pyramid Berkovich diamond nanoindenter was employed and measurement was done for five points of each film and the results were averaged. For minimization of substrate effect, a 75 μN load was used for penetration to prevent a penetration depth exceeding 10–15% of layer thickness. Measured values of the hardness and elastic modulus of the deposited Ti–W–N thin films were plotted in Fig. 7 as a function of RF power. As shown in this figure, Ti–N film has the lowest hardness and elastic modulus equal to 13.9 GPa and 272.1 GPa, respectively, which are comparable to the data reported in the literature [40–42]. Low hardness of this film can be due to several factors. First, low density and the presence of voids between the grains [43] as can be seen from SEM and cross-sectional micrographs. Second, low crystalline quality; this film shows a broad and low intensity XRD peak. Third, preferred orientation of (200); TiN_x is an anisotropic, and the hardness (H) changes in different orientations, where $H_{(111)} > H_{(200)}$. Therefore, if the Ti–N film had the (111) preferred orientation, it could have a higher hardness [26, 44]. Lower grain sizes compared with other prepared films do not play a significant role in the mechanical properties of this film.

In an RF power of 35 W and adding W to the Ti–N structure, it is clearly seen that the hardness of the films increases significantly, i.e., to 22.5 GPa. As mentioned above, by increasing RF power, some of the Ti atoms are replaced by W atoms and form a substitutional solid solution [17, 45]. On the other hand, by increasing W content in the film, the covalent level of the bonds increases and the columns attract each other with a larger force. As a result, the distance between the columns decreases and films will be denser and more compact, which will improve the hardness of the film. With regard to the difference between the lattice parameters, incorporation of W to Ti–N lattice leads to a distortion of the lattice which can alter internal stresses level and be a factor in increasing the hardness of the film [20]. By increasing RF power to 50 W, hardness decreases to 19.5 GPa, while the elastic modulus increases to 350.6 GPa, which can be related to the variation of the lattice strain (Table 2) and dominant phase and the texture coefficient of the film (Fig. 2). With further increase in RF power to 80 W, hardness rises again. The increase of elastic modulus with increasing RF power indicates the improvement of elasticity of the films by increasing W content. Furthermore, as RF power increases (> 50 W), the preferred orientation of the films was varied from (200) to (111), and it is well-known

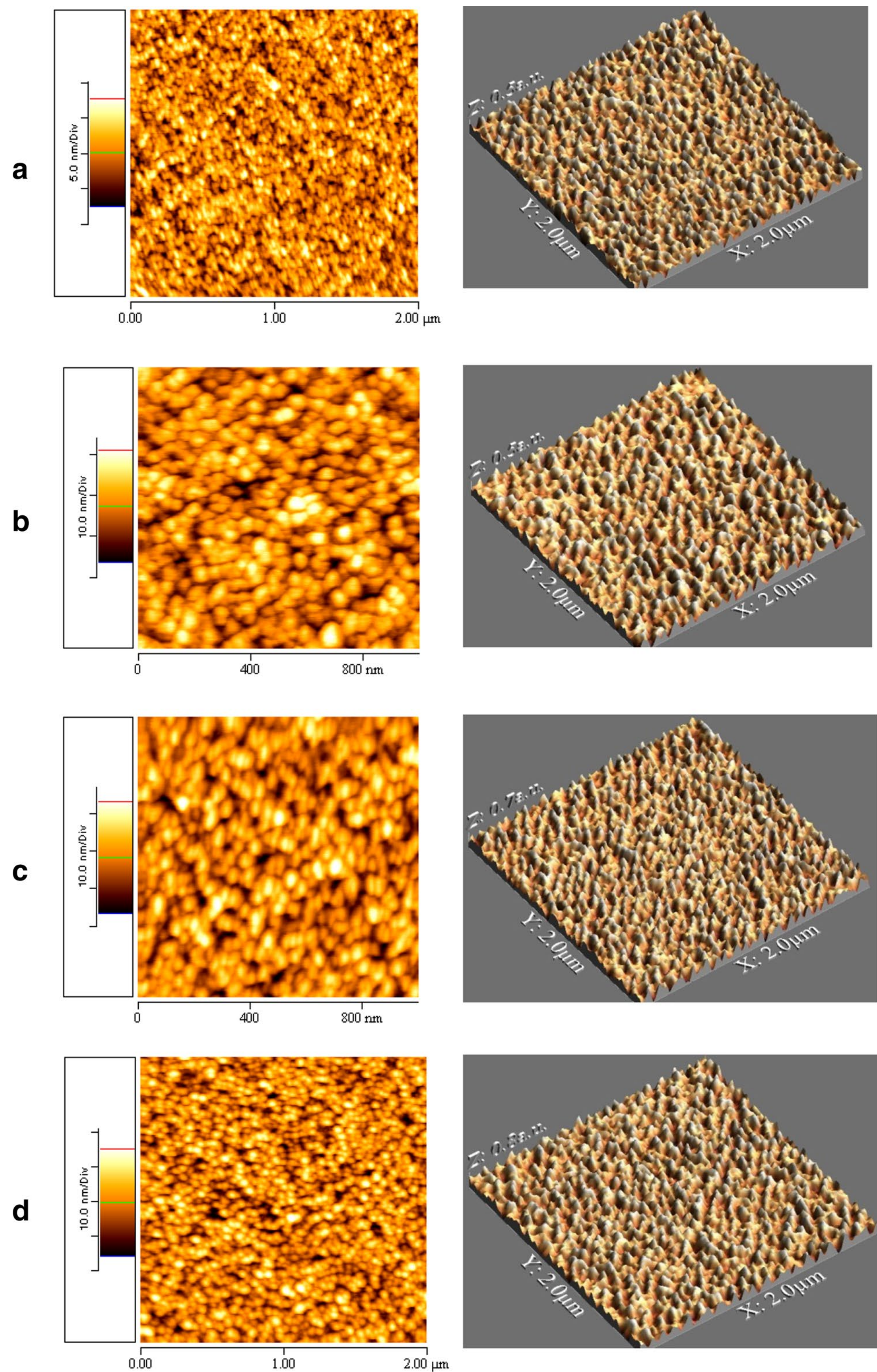

Fig. 5 2D & 3D AFM micrographs of prepared Ti–W–N thin films with different RF powers. **a** 0, **b** 35, **c** 50, **d** 100 W

that in fcc lattices the (111) plane is the most densely packed. Therefore, the development of (111) orientation can improve the density and thus the hardness of the films [46]. On the other hand, the presence of W atoms delocalizes the high concentration of electrons surrounding the nuclei, in Ti–N system, in the regions between the nuclei which result in translating the strong ionic character of Ti–N bonds into significantly more pronounced covalent character of W–N bonds in Ti–W–N compound [47]. Levy et al. [48] was reported that the replacement of Ti by W atoms increases the number of valence electrons at the Fermi level too and can dramatically modify the hardness of the films which is in agreement with this work's

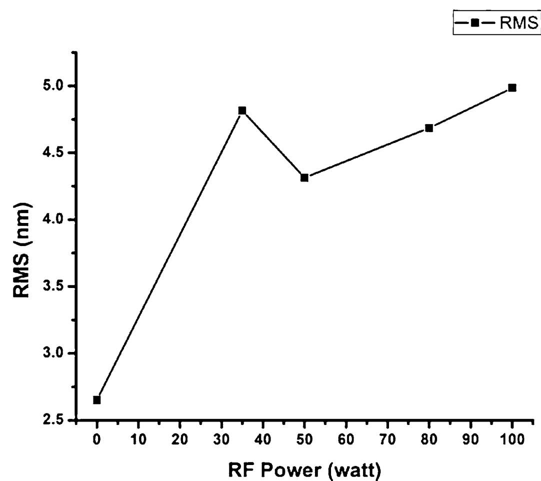

Fig. 6 RMS of Ti–W–N thin films with different RF powers

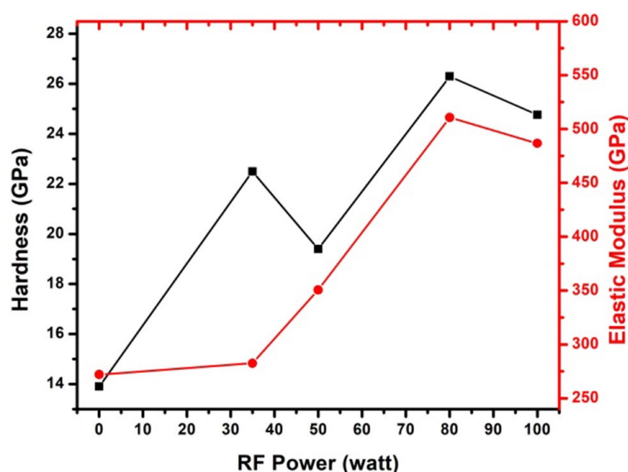

Fig. 7 Hardness and elastic modulus of Ti–W–N thin films at different RF powers

results. Finally, a further increase in RF power to 100 W results in a decrease in hardness and elastic modulus, which can be attributed to sub-stoichiometric property (N/(Ti + W) = 0.34) and the presence of high-density pores and cracks in the microstructure (Fig. 4d). All values obtained for hardness and elastic modulus are in good agreement with the literature data [5, 12, 17]. The maximum hardness (~ 26.5 GPa) and elastic modulus (~ 510 GPa) were obtained for the film deposited with 80 W RF power.

4 Conclusions

In this work, we investigated the effect of W concentration on the properties of Ti–W–N thin films deposited on glass and 304 steel substrates at a temperature of 150 °C. XRD measurements which showed that all films have fcc NaCl structure, and their preferred orientation transition are shifted from (200) for W < 39.9 at% to (111) for W ≥ 39.9 at%. The obtained results from XRD, FE-SEM, and atomic force microscopy (AFM) verified the increment of crystallinity, grain size and surface roughness by increasing the W content. Elemental composition investigation conducted with EDX indicated that the stoichiometry of the films is strongly affected by W concentration, where by increasing the RF power, and as a result, the W content, both Ti and N contents decrease, so that sub-stoichiometry characteristics of the films are increased. This can be due to low affinity of W for N compared to Ti for N. Furthermore, FE-SEM and cross-sectional images of the films represent columnar growth, and by increasing the W content in their structure, they become denser. Also, electrical resistivity of the films decreases from 3 to 0.063 kΩ cm by increasing RF power from 0 to 100 W. Considering nanoindentation measurements, by increasing W percentage from 0 to 50.6 %, the hardness and elastic modulus of the films increase from 13.9 to 272.1 GPa to 26.3 and 510.6 GPa, respectively. However, further increase in W percentage decreases the values of the hardness and elastic modulus. It was found that solid solution hardening and substrate temperature have significant roles in variations of the mechanical properties of the Ti–W–N thin films. According to the conducted analyses, it can be concluded that Ti–W–N thin film prepared with 80 W RF power is the most appropriate film, from electrical, microstructural and mechanical viewpoints, for diffusion barrier application.

References

1. J.M. Oparowski, R.D. Sisson Jr., R.R. Biederman, The effects of processing parameters on the microstructure and properties of sputter-deposited TiW thin film diffusion barriers. Thin Solid Films. **153**, 313–328 (1987). https://doi.org/10.1016/0040-6090(87)90192-1
2. M. Fugger, M. Plappert, C. Schäffer, O. Humbel, H. Hutter, H. Danninger, M. Nowottnick, Comparison of WTi and WTi(N) as diffusion barriers for Al and Cu metallization on Si with respect to thermal stability and diffusion behavior of Ti. Microelectron. Reliab. **54**, 2487–2493 (2014). https://doi.org/10.1016/j.microrel.2014.04.016
3. A.J.M.N.A.G. Dirks, R.A.M. Wolters, On the microstructure-property relationship of W–Ti–(N) diffusion barriers. Thin Solid Films **193/194**, 201–210 (1990)
4. S. Zhou, W. Liu, H. Liu, C. Cai, Structural and electrical properties of Ti–W–N thin films deposited by reactive RF sputtering. Phys. Procedia. **18**, 66–72 (2011). https://doi.org/10.1016/j.phpro.2011.06.059
5. J.C. Caicedo, L. Yate, J. Montes, Improving the physicochemical surface properties on AISI D3 steel coated with Ti–W–N. Surf. Coat. Technol. **205**, 2947–2953 (2011). https://doi.org/10.1016/j.surfcoat.2010.11.005

6. B. Tian, W. Yue, Z. Fu, Y. Gu, C. Wang, J. Liu, Microstructure and tribological properties of W-implanted PVD TiN coatings on 316L stainless steel, Vacuum. 99 (2014) 68–75. https://doi.org/10.1016/j.vacuum.2013.04.019
7. L. Yu, J. Chen, H. Ju, H. Dong, H. Zhao, Influence of Al content on microstructure, mechanical and tribological properties of Ti–W–Al–N composite films. Vacuum. **137**, 31–37 (2017). https://doi.org/10.1016/j.vacuum.2016.11.004
8. V.F.B.L.R. Shaginyan, M. Misina, J. Zemek, J. Musil, F. Regent, Composition, structure, microhardness and residual stress of W–Ti–N films deposited by reactive magnetron sputteringle. Thin Solid Films **408**, 136–147 (2002)
9. E.K.A.N. Kuchuk, V.P. Kladko, V.F. Machulin, A. Piotrowska, Diffusion barrier properties of reactively sputtered W–Ti–N thin films, Rev. Adv. Mater. Sci. **8**, 22–26 (2004)
10. A.V.K.L.R. Shaginyan, Mechanisms for hardening film materials: W–Ti–N and TiN–Cu systems as examples. Powder Metall. Met. Ceram. **44**, 161–168 (2005)
11. D. Braga, J.P. Dias, A. Cavaleiro, Duplex treatment: W–Ti–N sputtered coatings on pre-nitrided low and high alloy steels. Surf. Coat. Technol. **200**, 4861–4869 (2006). https://doi.org/10.1016/j.surfcoat.2005.04.056
12. V. Severo, L. Vilhena, P.N. Silva, J.P. Dias, D. Becker, S. Wagner, A. Cavaleiro, Tribological behaviour of W–Ti–N coatings in semi-industrial strip-drawing tests. J. Mater. Process. Technol. **209**, 4662–4667 (2009). https://doi.org/10.1016/j.jmatprotec.2008.11.040
13. P. Homhuan, J. Pongsopa, Structural and mechanical properties of Ti–WN thin films by dual unbalanced magnetron sputtering, Adv. Mater. Res. 1131 (2015) 246–250. https://doi.org/10.4028/www.scientific.net/AMR.1131.246
14. C.W.J.H. Moser, F. Tian, O. Haller, D.B. Bergstrom, I. Petrov, J.E. Greene, Single-phase polycrystalline Til_xWxN alloys (0â©½ xâ©½ 0.7) grown by UHV reactive magnetron sputtering: microstructure and physical properties. Thin Solid Films. **253**, 445–450 (1994)
15. M.R. Baklanov, P.S. Ho, E. Zschech (eds.), Advanced interconnects for ULSI technology (Wiley, United Kingdom, 2012)
16. W. Qingxiang, L. Shuhua, W. Xianhui, F. Zhikang, Diffusion barrier performance of amorphous WTiN films in Cu metallization. Vacuum. **84**, 1270–1274 (2010). https://doi.org/10.1016/j.vacuum.2010.02.002
17. J.C. Caicedo, L. Yate, G. Cabrera, W. Aperador, G. Zambrano, P. Prieto, Effect of negative bias voltage on mechanical and electrochemical nature in Ti–W–N coatings. J. Mater. Sci. **46**, 1244–1252 (2011). https://doi.org/10.1007/s10853-010-4904-7
18. R.F. Londoño-Menjura, R. Ospina, D. Escobar, J.H. Quintero, J.J. Olaya, A. Mello, E. Restrepo-Parra, Influence of deposition temperature on WTiN coatings tribological performance. Appl. Surf. Sci. **427**, 1096–1104 (2018). https://doi.org/10.1016/j.apsusc.2017.07.215
19. N.D. Cuong, D.-J. Kim, B.-D. Kang, S.-G. Yoon, Effects of nitrogen concentration on structural and electrical properties of titanium nitride for thin-film resistor applications, Electrochem. Solid-State Lett. **9**, G279 (2006). https://doi.org/10.1149/1.2216592
20. M.T.V.A. Cavaleiro, B. Trindade, The influence of the addition of a third element on the structure and mechanical properties of transition-metal-based nanostructured hard films: part I—nitrides. Nanostructured Coatings, Springer, New York, 2006
21. A.V. Kuchuk, V.P. Kladko, O.S. Lytvyn, A. Piotrowska, R.A. Minikayev, R. Ratajczak, Relationship between condition of deposition and properties of W–Ti–N thin films prepared by reactive magnetron sputtering. Adv. Eng. Mater. **8**, 209–212 (2006). https://doi.org/10.1002/adem.200500263
22. N.W.A.A.R. Denton, Vegard's law. Phys. Rev. A **43**, 3161–3164 (1991)
23. J.P. Zhao, X. Wang, Z.Y. Chen, S.Q. Yang, T.S. Shi, X.H. Liu, Overall energy model for preferred growth of TiN films during filtered arc deposition. J. Phys. D Appl. Phys. **30**, 5–12 (1997). https://doi.org/10.1088/0022-3727/30/1/002
24. M. Popović, M. Novaković, M. Mitrić, K. Zhang, N. Bibić, Structural, optical and electrical properties of argon implanted TiN thin films. Int. J. Refract. Met. Hard Mater. **48**, 318–323 (2015). https://doi.org/10.1016/j.ijrmhm.2014.09.026
25. N.K. Ponon, D.J.R. Appleby, E. Arac, P.J. King, S. Ganti, K.S.K. Kwa, A. O'Neill, Effect of deposition conditions and post deposition anneal on reactively sputtered titanium nitride thin films. Thin Solid Films. **578**, 31–37 (2015). https://doi.org/10.1016/j.tsf.2015.02.009
26. G. Martinez, V. Shutthanandan, S. Thevuthasan, J.F. Chessa, C.V. Ramana, Effect of thickness on the structure, composition and properties of titanium nitride nano-coatings. Ceram. Int. **40**, 5757–5764 (2014). https://doi.org/10.1016/j.ceramint.2013.11.014
27. N. Arshi, J. Lu, Y.K. Joo, C.G. Lee, J.H. Yoon, F. Ahmed, Study on structural, morphological and electrical properties of sputtered titanium nitride films under different argon gas flow. Mater. Chem. Phys. **134**, 839–844 (2012). https://doi.org/10.1016/j.matchemphys.2012.03.078
28. M.L. Addonizio, A. Castaldo, A. Antonaia, E. Gambale, L. Iemmo, Influence of process parameters on properties of reactively sputtered tungsten nitride thin films. J. Vac. Sci. Technol. A Vac. Surf. Film. **30**, 31506 (2012). https://doi.org/10.1116/1.3698399
29. M. Wen, Q.N. Meng, W.X. Yu, W.T. Zheng, S.X. Mao, M.J. Hua, Growth, stress and hardness of reactively sputtered tungsten nitride thin films. Surf. Coatings Technol. **205**, 1953–1961 (2010). https://doi.org/10.1016/j.surfcoat.2010.08.082
30. C. Gu, Z. Sui, Y. Li, H. Chu, S. Ding, Y. Zhao, C. Jiang, The growth of the metallic ZrN x thin films on P-GaN substrate by pulsed laser deposition. Appl. Surf. Sci. **433**, 306–311 (2018). https://doi.org/10.1016/j.apsusc.2017.09.262
31. H. Guo, W. Chen, Y. Shan, W. Wang, Z. Zhang, J. Jia, Microstructures and properties of titanium nitride films prepared by pulsed laser deposition at different substrate temperatures. Appl. Surf. Sci. **357**, 473–478 (2015). https://doi.org/10.1016/j.apsusc.2015.09.061
32. R. Jalali, M. Parhizkar, H. Bidadi, H. Naghshara, S.R. Hosseini, M. Jafari, Effect of Al content, substrate temperature and nitrogen flow on the reactive magnetron co-sputtered nanostructure in TiAlN thin films intended for use as barrier material in DRAMs. J. Korean Phys. Soc. **66**, 978–983 (2015). https://doi.org/10.3938/jkps.66.978
33. R.E. Bunshah (ed), Handbook of hard coatings: deposition technologies, properties and applications. (Noyes Publications, Norwich, 2001)
34. X.X. Zhang, Y.Z. Wu, B. Mu, L. Qiao, W.X. Li, J.J. Li, P. Wang, Thermal stability of tungsten sub-nitride thin film prepared by reactive magnetron sputtering. J. Nucl. Mater. **485**, 1–7 (2017). https://doi.org/10.1016/j.jnucmat.2016.12.009
35. S.T. Alu, S. Stach, S. Valedbagi, S.M. Elahi, R. Bavadi, Surface morphology of titanium nitride thin films synthesized by DC reactive magnetron sputterin. Mater. Sci. **33**, 137–143 (2015). https://doi.org/10.1515/msp-2015-0010
36. A. Lahav, K.A. Grim, I.A. Blech, Measurement of thermal expansion coefficients of W, WSi, WN, and WSiN thin film metallizations. J. Appl. Phys. **67**, 734–738 (1990). https://doi.org/10.1063/1.345779
37. N.P. Bansal, R.H. Doremus, Handbook of glass properties, Handb. Glas. Prop. (2013) 1–680. https://doi.org/10.1016/C2009-0-21785-5

38. Y.R. Luo, Comprehensive handbook of chemical bond energies. CRC press 2007
39. S.S. Firouzabadi, K. Dehghani, M. Naderi, F. Mahboubi, Numerical investigation of sputtering power effect on nano-tribological properties of tantalum-nitride film using molecular dynamics simulation. Appl. Surf. Sci. **367**, 197–204 (2016). https://doi.org/10.1016/j.apsusc.2015.12.075
40. K. Khojier, M. Jafarzadeh, H. Savaloni, Z. Dehghani, N. Zare Dehnavi, Influence of argon gas flow on mechanical and electrical properties of sputtered titanium nitride thin films. J. Theor. Appl. Phys. **7**, 37–42 (2013). https://doi.org/10.4028/www.scientific.net/AMR.829.497
41. A.N. Wang, J.H. Huang, H.W. Hsiao, G.P. Yu, H. Chen, Residual stress measurement on TiN thin films by combing nanoindentation and average X-ray strain (AXS) method, Surf. Coatings Technol. **280**, 43–49 (2015). https://doi.org/10.1016/j.surfcoat.2015.08.059
42. J.C. Oliveira, F. Fernandes, R. Serra, A. Cavaleiro, On the role of the energetic species in TiN thin film growth by reactive deep oscillation magnetron sputtering in Ar/N2. Thin Solid Films. **645**, 253–264 (2018). https://doi.org/10.1016/j.tsf.2017.10.052
43. P. Patsalas, C. Charitidis, S. Logothetidis, The effect of substrate temperature and biasing on the mechanical properties and structure of sputtered titanium nitride thin films. Surf. Coatings Technol. **125**, 335–340 (2000). https://doi.org/10.1016/S0257-8972(99)00606-4
44. S.V. Hainsworth, W.C. Soh, The effect of the substrate on the mechanical properties of TiN coatings, Surf. Coatings Technol. 163–164, 515–520 (2003). https://doi.org/10.1016/S0257-8972(02)00652-7
45. G.Z. Junhua Xu, H. Luo, H. Ju, L. Yu, Microstructure, mechanical and tribological properties of TaWN composite films. Vacuum. **146**, 246–251 (2017)
46. R.G. Elliman, M.C. Ridgway, Ion beam modification of materials. Elsevier, Amsterdam (1996)
47. D. Sangiovanni, V. Chirita, L. Hultman, Electronic mechanism for toughness enhancement in Ti x M 1-x N (M = Mo and W), Phys. Rev. B (2010) 10. https://doi.org/10.1103/PhysRevB.81.104107
48. P. Hones, P.E. Schmid, R. Sanjine, M. Diserens, C. Wiemer, F. Le, Electronic states and mechanical properties in transition metal nitrides. Surf. Coat. Technol. **121**, 284–290 (1999)